Int. J. Heat Mass Transfer. Vol. 31, No. 11, pp. 2239–2249, 1988
Printed in Great Britain

0017–9310/88 $3.00+0.00

Heat and momentum transfer in laser induced decomposition of silane jets: theory and experiments

I. S. AKMANDOR
Department of Aeronautical Engineering, Middle East Technical University, Inonu Blvd., Ankara, Turkey

and

J. SZEKELY and J. S. HAGGERTY
Department of Material Science and Engineering, Massachusetts Institute of Technology, 77 Massachusetts Avenue, Cambridge, MA 02139, U.S.A.

(*Received* 22 *September* 1987 *and in final form* 26 *January* 1988)

Abstract—Silicon powders are obtained by laser pyrolysis of silane gas. Temperature and velocity profiles are determined both theoretically and experimentally. The velocimetry consists of a marker technique which measures the propagation time of a perturbation front through the hot reaction zone. In the theoretical model, the coaxial jet expansion undergoing a thermal heating is studied by defining a Dorodnitzin–Illingworth transformation. The results show a decrease of axial velocity as the gas enters the laser heated region. The change is sharper for higher inlet velocities. In this region, the gradients of the axial temperature profiles are high.

1. INTRODUCTION

THE PURPOSE of this investigation was to develop an improved fundamental understanding of the laser induced decomposition of silane gas to yield a nearly monodispersed fine silicon powder. The production of such a material is of considerable interest at present due to its possible application in the manufacture of silicon carbide or silicon nitride for use as components in the fabrication of structural ceramics [1–4]. The generation of a monodispersed powder is an essential requirement and the design of a successful reaction system will require a good quantitative understanding of the heat flow and fluid flow aspects of this system. Hence this paper will mainly focus on the velocity and temperature fields in a laboratory-scale reactor used for producing such powders.

The decomposition reaction of silane proceeds according to the following relationship:

$$SiH_4(g) \rightarrow Si(s) + 2H_2(g). \quad (1)$$

The silane is heated by absorbing infra-red photon energy emitted by a CO_2 laser.

The work to be described has three principal components.

(1) Experimental measurements to determine the temperature and velocity profiles of the reaction system.

(2) An asymptotic analytical description of the system.

(3) A comparison of the theoretical model with the measurements.

2. EXPERIMENTAL

Figure 1 shows a schematic sketch of the experimental arrangement. It is seen that silane gas, surrounded by a coaxial argon stream is injected into a reaction chamber. The silane stream is exposed to a CO_2 laser beam, producing a high-temperature reaction zone. A detailed drawing of the assembly is given in Fig. 2. Typical operating conditions are listed in Table 1. During this process, 2.78% of the 180 W laser power is absorbed and almost 100% of the silane gas is converted to submicrometer silicon powder.

Clearly this is a highly complex reaction system, the detailed representation of which would require knowledge of not only the heat flow and fluid phenomena in the system but also of the nucleation and coalescence kinetics, pertaining to the solid product. For the

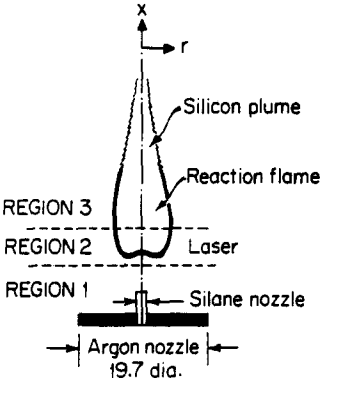

FIG. 1. Geometry of the problem.

NOMENCLATURE

A cross-sectional area of the reaction zone
$a_0, a_1, a_2, \ldots$ constants in the temperature equation for region 1
$C_0, C_1, C_2, C_3, C_4, C_5, C_6$ integration constants determined by patching corresponding subregions
C_7 constant, $2\pi hc^2$
C_8 constant, ch/K_b
c velocity of light
C_p specific heat
D diameter of the incident laser beam
$g(\eta)$ non-dimensional stream function
Gr Grashof number
ΔH heat of reaction
h Planck constant
$J_0(\ ), J_{1/2}(\ )$ Bessel functions
K first-order reaction rate
K_b Boltzmann constant
L length scale: average flame width
ΔL axial length of the absorbing volume
$\dot{m}$ mass flow rate
P_0 incident laser power
p, P pressure
Q mass flux
q absorbed energy source density
q_0 incident energy source density
STP standard temperature (20°C) and pressure (1 atm)
R silane nozzle radius
R_0 radius at which $u_1(R_0) = u_2(R_0) : R_0$ is found by equating $du_1/dr|_{r=R_0} = du_2/dr|_{r=R_0}$
$r, \bar{r}$ radius and radius corrected for temperature variation, respectively
S brightness temperature
$T, T(x, r)$ local temperature
T_{ref} reference temperature
T_w wall temperature
Δt time interval taken by a particle to travel between two laser probe beams
$u, \bar{U}$ local and averaged silane velocity: subscript 1, refers to Poiseuille profile; 2, refers to Squire profile; 'ar' refers to argon velocity
v radial velocity component
W_λ chromatic emissive power
X axial length scale
Δx distance (1 mm) between two laser probe beams.

Greek symbols

α thermal diffusivity
α_{abs} laser absorption coefficient
β coefficient of thermal expansion
ε emissivity
η non-dimensional independent variable
$\theta_0(r), \theta_1(r), \theta_2(r)$ functions associated with the radial distribution of the temperature in the pre-heated region
κ thermal conductivity
λ wavelength
μ viscosity
ν kinematic viscosity
π 3.141592654
ρ density
σ Stefan–Boltzmann constant
τ reaction time.

present we shall confine our attention to determining the velocity and the temperature fields because this information is a necessary requirement in performing nucleation and coalescence studies. The rate of thermal decomposition of silane is thought to be fast compared to the rate of convection, justifying the decoupling of the kinetics from the fluid flow and heat transfer phenomena.

3. VELOCITY MEASUREMENTS

Velocity measurements in the high-temperature reaction system are quite difficult to perform. In the present case, the use of laser-Doppler velocimetry was attempted but was unsuccessful because fine (10–30 nm) silicon particles were present. In the present work, two complimentary techniques were employed.

(1) Velocity estimate using a marker technique.

(2) Velocity estimate from the width of the reaction zone.

3.1. *The marker technique*

3.1.1. *Description of the technique.* This technique involves the introduction of a 'marker' in the flow. The generation of such a marker within the reaction zone is achieved by chopping the main laser beam for 0.8 ms (Figs. 3 and 4). The disturbance is long enough to locally stop the silicon nucleation process. However, it is still of small magnitude and does not affect the overall structure of the flame-like region. The disturbance causes a front across which the particle number density is low; the location of the front is detected by using a He–Ne laser beam as a probe and analyzing the intensity of the beam transmitted through the reaction zone. This front is convected toward the chimney (Fig. 2) at the local velocity.

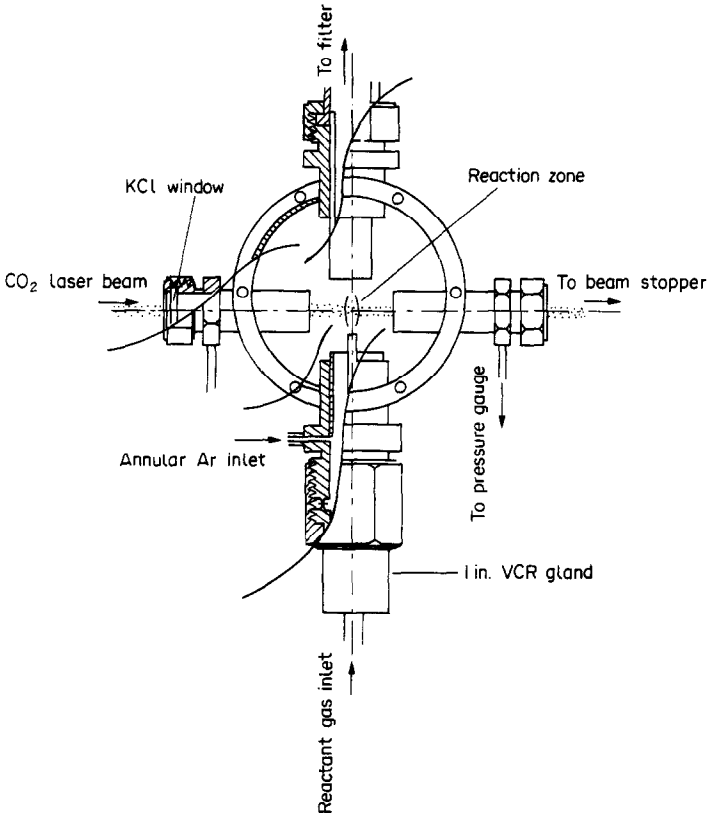

FIG. 2. Detailed drawing of the assembly.

The time such a marker takes to travel between two predetermined points (A and B in Fig. 3) gives the average local velocity

$$V = \frac{\Delta x}{\Delta t}. \quad (2)$$

Generating such a marker without disturbing the entire reaction zone is only possible if the chemical reaction time is much faster than the convection time. For this purpose the following time scales have been identified.

(a) A convection time scale (D/U) which is based on the diameter D ($\simeq 1$ mm) of the incident laser beam and the local average gas velocity U ($\simeq 1$ m s^{-1}). This is the average residence time within the laser heated region. Hence, the convection time scale is of the order of 1 ms.

(b) A conduction time scale ($D^2/4\alpha$) which is based

Table 1. Flow and synthesis characteristics

	Figure number	Cell pressure (atm)	Silane mass flux (cm^3 min^{-1}) STP
Axial velocity profiles	6	upper: 0.2	38
		lower: 0.7	30
Axial temperature profiles	7	0.7	30
		0.7	38
		0.2	38
Radial velocity profiles	8	0.2	38
Radial temperature profiles	9	0.2	38
Temperature map of the reaction zone	10	0.2	38

Incident laser profile is Gaussian.
Silane nozzle diameter is 1.19 mm.
Argon nozzle diameter is 19.70 mm.
The Reynolds number belongs to the silane flow at the nozzle inlet.
The Grashof number belongs to the flow at the jet centerline.
Run 1: flow at 38.00 cm^3 min^{-1} (0.2 atm); Reynolds number, 51.80; Grashof number, 2.73.
Run 2: flow at 30.00 cm^3 min^{-1} (0.7 atm); Reynolds number, 40.90; Grashof number, 5.07.

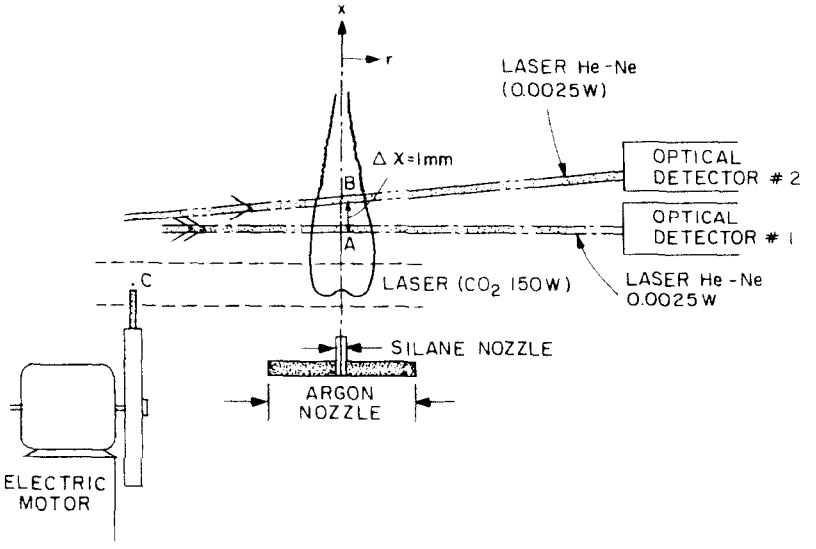

FIG. 3. Side view of the set-up for velocity measurements.

on the thermal diffusivity α and a typical length scale (D, laser diameter). The conduction time scale was also found to be of the order of 1 ms.

(c) A reaction time scale $(1/K)$ where K is the following specific reaction rate constant [5]:

$$K = 5.0 \times 10^{12} \exp[218\,196(\mathrm{J\,mol^{-1}})/RT]. \quad (3)$$

This rate corresponds to the initial dissociation step of the overall silane pyrolysis

$$SiH_4 \rightarrow SiH_2 + H_2. \quad (4)$$

In the dimensional analysis described here, the order of the rate determining step was assumed to be 1 and the typical reaction time was found to be [6]

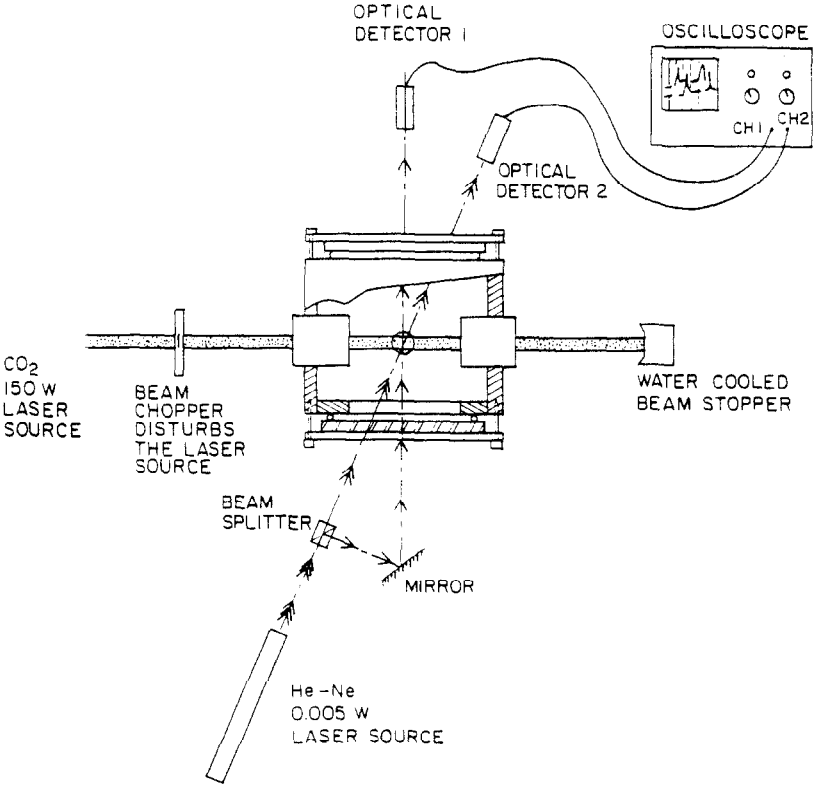

FIG. 4. Top view of the set-up for velocity measurements.

$$\tau = \frac{\ln 2}{K} = 5.8 \times 10^{-6}\,\text{s}. \quad (5)$$

This scale analysis shows that the chemical reaction is some 1000 times faster than heat transfer by convection or conduction. It should be noted that the marker method does not measure the velocity of the gas flow but the velocity of the disturbance front. Therefore, the main assumption is that the velocity at which the front propagates is equal to the local gas velocity. The front is composed of spherical silicon particles which have very small (10–30 nm) sizes and low drag coefficients. As these particles are entrained in the flow, the velocity of the gas–solid mixture and the disturbance front are equal.

3.1.2. *The experimental arrangement for the marker technique.* The equipment given below was used in the velocity measurements.

(a) A 180 W laser source: Coherent Everlase Model 150 which was the main source of power to be perturbed.

(b) A He–Ne 0.005 W laser the beam of which was split and used as two probe beams located at different axial locations.

(c) A 50–50% beam splitter.

(d) Two highly sensitive photodetectors which were used to collect the transmitted He–Ne probe beams.

(e) A circular plate fixed around the reaction cell and which carried the probe laser source and the photodetectors.

(f) A beam chopper with a variable speed (0–4000 r.p.m.).

The top view of the experimental arrangement is given in Fig. 4. A low-power (0.005 W) He–Ne laser was used as the source of two synchronized beams. Each of these beams was directed toward the flame centerline at slightly different axial locations. The distance between them was set to 1 mm and was not changed during the experiments. The probe laser source and the photodetectors were carried on a support plate. This eliminated the need for successive alignments as the probes were displayed along the jet centerline.

3.1.3. *Summary of the marker technique.* This technique has the characteristics given below.

(a) No probes are physically inserted into the flow.

(b) The transmitted He–Ne beam is analyzed instead of the scattered light. The latter is much weaker due to the dense reaction zone.

Figure 5 displays the output of photodetectors recording the signature of the disturbance front as it passes through the probe He–Ne laser beams. The top two oscilloscope displays on this figure illustrate the difference between a strong disturbance causing the periodic oscillation of the reaction region and a lighter disturbance. The frequency of the chopping blade was $1/12\ \text{s}^{-1}$ during the experimental runs and the duration of each disturbance was 8.0×10^{-4} s. This was slightly less than typical convection or conduction times. Because the probing beams were placed 1 mm from each other, a time lapse Δt was required for the perturbation front to clear the first beam and reach the second one. By inspecting these photographs (Fig. 5), it can be seen that the time interval Δt increases as the probing pair of laser beams are located further away from the inlet nozzle. This shows that the velocity of the gas is decreasing. The axial velocity obtained from this method is shown in Fig. 6.

3.2. *Velocity estimate from the width of the reaction zone*

The second experimental curve of velocity values plotted on the same graph (Fig. 6) was obtained by using the following continuity relationship:

$$\dot{m} = \rho U A \quad (6)$$

where A is the cross-sectional area of the reaction zone at each axial location determined from a photograph. The density ρ has been estimated from the axial temperature distribution (Fig. 7). The experimental temperatures were measured with an optical pyrometer which determines the intensity of the absolute emittance of light. This technique is widely used in combustion and flame research. The details of the method as applied to the silane pyrolysis have been given in ref. [7] but a brief description is given in Section 4. The following assumptions were made.

(a) The cell pressure is constant in the entire cell.

(b) The radial and axial species concentrations are known so that the local composition of the gas mixture is known (or can be estimated).

(c) The gas mixture follows the ideal law.

Once the density ρ, and the axial cross-sectional area A are known, the average velocities U at different axial locations can be determined from equation (6). The volume of flow which increases with distance x from the silane inlet due to mixing with argon can also be taken into account if the following equation [8] is used:

$$\dot{m}/\rho = Q = 8\pi\nu x. \quad (7)$$

The centerline velocity is then calculated by assuming a Gaussian radial velocity profile. This simple calculation is in fair agreement with the marker technique. A major disadvantage of this simple calculation is that the local density of the reacting gas must be known beforehand. Figure 6 shows the experimental velocity profiles. The comparison of these with theoretical predictions will be presented later in this paper.

4. TEMPERATURE MEASUREMENTS IN THE REACTION ZONE

The temperature data along the axis of the reaction zone were measured by an optical pyrometer. The data are shown in Fig. 7 and the error of the measurements estimated to be less than 3% of the plotted values.

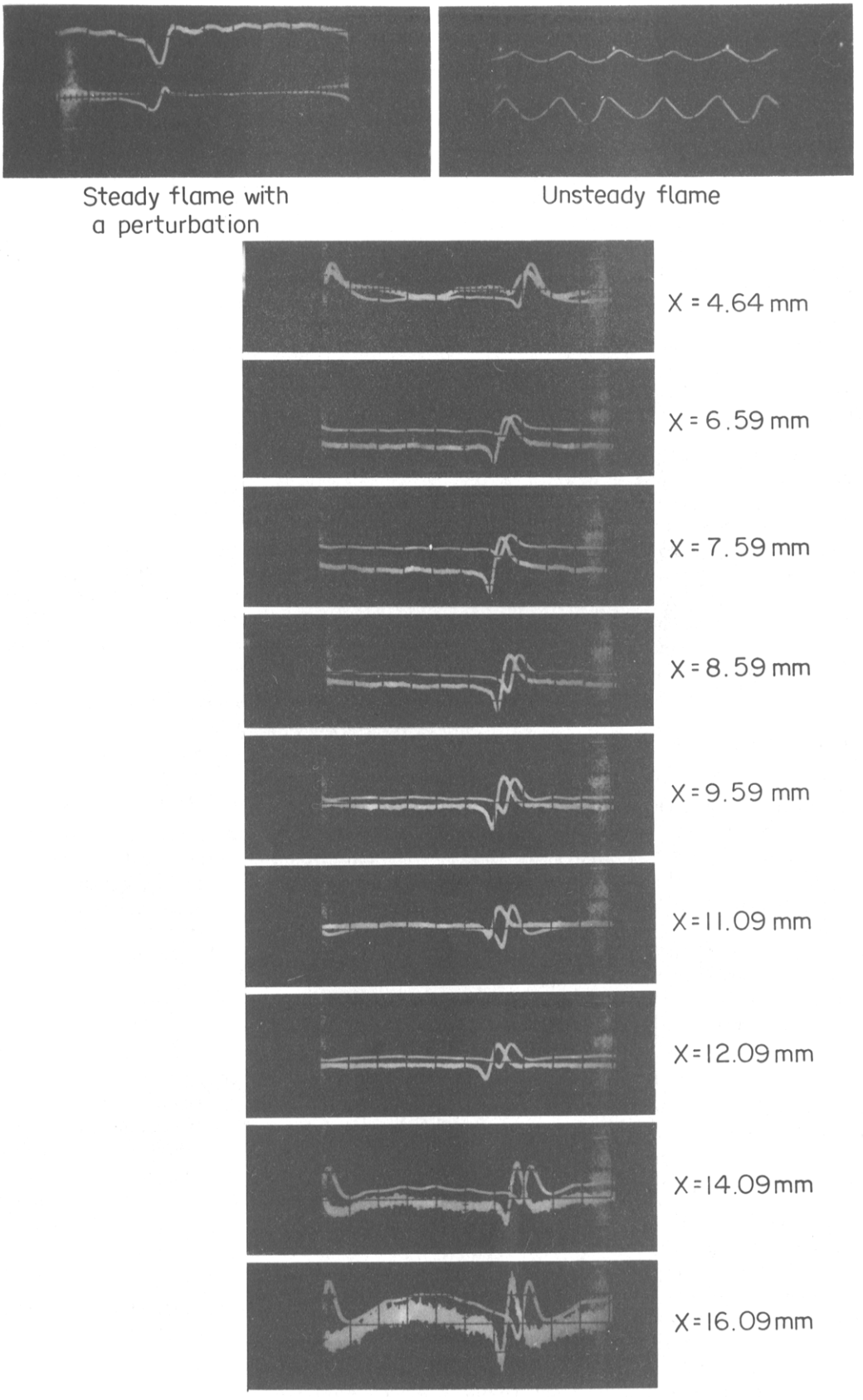

FIG. 5. Signal displayed by the photodetectors: propagation of the disturbance front at different axial locations.

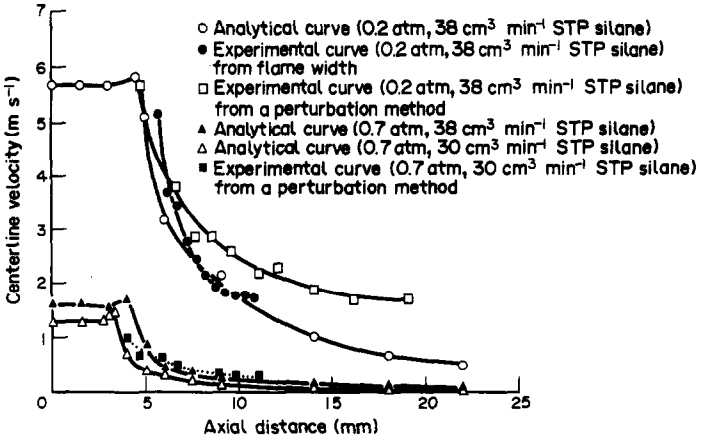

FIG. 6. Axial velocity profiles.

The experimental temperature in the silicon reaction flame ranges from 1000 to 1400 K for the conditions shown in Table 1. The silicon particles nucleate after the thermal decomposition of the silane gas and radiate in the visible spectrum thus creating a hot flame-like region. The radiation is collected by the pyrometer from a probing area having a diameter of less than 2 mm. The instrument measures the monochromatic emissive power W_λ and the brightness temperature S is obtained from the following formula:

$$W_\lambda = \frac{C_7 \lambda^{-5}}{e^{C_8/\lambda S}}. \tag{8}$$

The temperature T of the probe volume is calculated from

$$\frac{1}{T} = \frac{1}{S} + (\lambda \ln \varepsilon)/C_8 \tag{9}$$

where the emissivity ε of the dense silicon cloud was determined by experiment and theoretical Mie calculations [7].

5. ANALYSIS

In the analysis presented here, an asymptotic approach is used which will enable us to obtain essentially closed form solutions for the velocity and temperature fields in the silicon powder reactor. The assumptions made in order to achieve an analytical solution, though somewhat restrictive, are thought to be reasonable. A more comprehensive numerical approach to this problem will be presented in a subsequent paper.

5.1. *Introduction to the analytical asymptotic approach*

For the purpose of analysis, the system has been subdivided into three regions as shown in Fig. 1.

(1) The preheat region, upstream of the laser beam.
(2) The reaction region mainly in the laser beam.
(3) The post-reaction region after the laser beam.

Slightly different equations will be employed to represent these regions because the influence of convec-

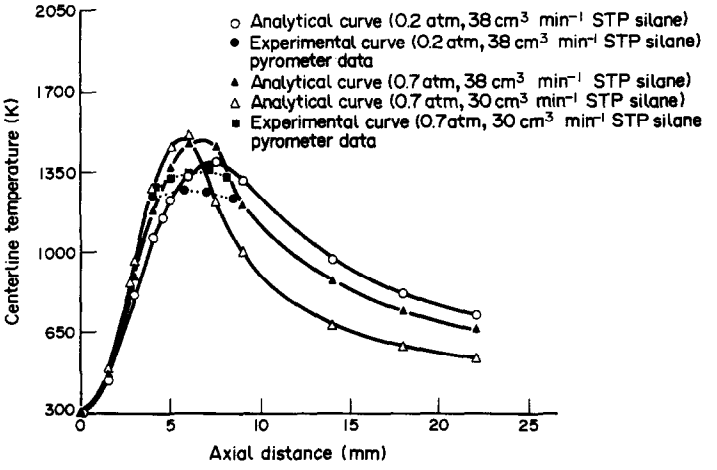

FIG. 7. Axial temperature profiles.

tion, diffusion, radiation and other source terms is different upstream of the reaction zone, in the reaction zone and downstream of it. By neglecting the lower order terms in these subregions, it is possible to integrate the governing equations of mass, momentum, energy and then patch them at the boundaries of the subregions to obtain a closed form solution over the whole domain.

5.2. *Assumptions*

(a) The reaction zone diameter (0.7 cm) is assumed to be small when compared to the powder cell diameter (7.62 cm). Thus wall effects on the reaction flame shape have been neglected.

(b) The silane reaction is weakly exothermic and the heat released from the reaction is weakly exothermic and the heat released from the reaction is neglected (0.36 W) after comparing it with the absorbed laser power (5.0 W).

(c) The decomposition rate of silane is assumed to be infinite because the chemical reaction time has already been shown to be some 1000 times smaller than the convection time.

(d) The threshold temperature at which the temperature decomposition occurs is assumed to be 600°C. Furthermore, the sudden volume changes due to the temperature and the reaction have been assumed to affect primarily the density of the reaction zone without having a substantial impact on the cell pressure.

(e) This is a low Reynolds number flow and the silicon particles are assumed to move at the local gas speed [9]. Hence the problem is treated as that of a single phase, multicomponent system.

5.3. *Equations and closed form solutions*

5.3.1. *Region* 1 : *The preheated region, upstream of the reaction zone.* The equations governing the velocity in region 1 are listed below.

Mass equation

$$\frac{\partial u}{\partial x} = 0. \tag{10}$$

Momentum equation

$$\frac{v}{r}\left(\frac{\partial}{\partial r}\left(r\frac{\partial u}{\partial r}\right)\right) = \frac{1}{\rho}\frac{\mathrm{d}p}{\mathrm{d}x}. \tag{11}$$

Boundary conditions

$$u(\infty) = \bar{U}_{\mathrm{ar}}; \quad \left.\frac{\partial u}{\partial r}\right|_{r=0} = 0. \tag{12}$$

Velocity profiles

Poiseuille profile

$$u_1(r) = 2\bar{U}\left(1-\left(\frac{r}{R}\right)^2\right), \quad r \leqslant R_0$$

Squire profile

$$u_2(r) = C_0\frac{v}{r} + \bar{U}_{\mathrm{ar}}, \quad r \geqslant R_0.$$

The axial length of this region is about 5–10 times the diameter of the silane nozzle. In region 1, the similarity assumption does not hold since the jet is developing and the core region still persists. For most of region 1, the Poiseuille profile at the inlet can be a fair approximation and is adopted here. For a large radius r, this solution is not valid as the velocity values are negative. The far field solution is obtained by patching the Poiseuille solution to the solution obtained by Squire [10].

The energy equation for the preheat region is given below.

Energy equation

$$\rho C_p \bar{U}\frac{\partial T}{\partial x} = \frac{\partial}{\partial x}\left(\kappa\frac{\partial T}{\partial x}\right) + \frac{\partial}{r\,\partial r}\left(\kappa r\frac{\partial T}{\partial r}\right). \tag{13}$$

Boundary conditions

$$T(0,r) = T_{\mathrm{w}}, \quad T(x,\infty) = T_{\mathrm{w}}, \quad \left.\frac{\partial T}{\partial r}\right|_{r=0} = 0.$$

Assumed profile

$$T(x,r) = T_0 + a_0\Theta_0(r) + a_1\Theta_1(r)x + a_2\Theta_2(r)x^2 + \cdots \tag{14}$$

Temperature solution

$$T(x,r) = C_1\left(x + \frac{\bar{U}}{\alpha}x^2\right)J_0\left(\frac{\bar{u}}{\alpha}r\right) + T_{\mathrm{w}} \tag{15}$$

valid for

$$\frac{u}{\alpha}r \leqslant 0.3.$$

The axial part of the series expansion can also be obtained by separation of variables [11]. The present analysis only calculates the leading order solution of the temperature fields. The complete solution would probably be in terms of a summation of Bessel functions. Superposition of such functions would then eliminate the oscillation which is present as r goes to infinity.

5.3.2. *Region* 2: *The reaction zone.* The Navier–Stokes equations and solutions corresponding to region 2 are given below.

Mass

$$\frac{\partial}{\partial x}(\rho u r) + \frac{\partial}{\partial r}(\rho v r) = 0. \tag{16}$$

Momentum

$$\rho u\frac{\partial u}{\partial x} + \rho v\frac{\partial u}{\partial r} = \frac{\mu\partial}{r\,\partial r}\left(r\frac{\partial u}{\partial r}\right) + \rho g\beta\Delta T \tag{17}$$

$$u = \frac{vg'}{x\eta}, \quad g'(\eta) = \frac{\mathrm{d}g}{\mathrm{d}\eta}, \quad \eta = \frac{\bar{r}}{x}. \tag{18}$$

Here $\bar{r}$ is defined by the Dorodnitzyn–Illingworth transformation

$$\bar{r} = \left(2\int_0^r \frac{\rho}{\rho_\infty} r\,\mathrm{d}r\right)^{1/2} \tag{19}$$

$$g(\eta) = \frac{C_2\left(\eta^2 - \frac{Gr}{128}\eta^6\right) - \frac{Gr}{16}\eta^4}{C_2\left(\frac{\eta^2}{4} - \frac{Gr}{1536}\eta^6\right) + 1 - \frac{Gr}{16}\eta^4} \tag{20}$$

valid for

$$\frac{Gr^{1/2}\eta^2}{8} < 0.175.$$

The length of this region is determined by the diameter of the horizontally impinging laser beam. In this region, the self similarity of the jet is assumed and a Dorodnitzyn–Illingworth transformation has been used to take into account the gas expansion due to heating. This transformation allows the density of the gas to be dependent on the temperature, and at the same time, decouples the momentum equation from the energy equation. However, this is an approximate formulation since the viscous term on the right-hand side of the momentum equation is not transformed exactly. This method gives relatively good results especially if the *radial* density gradients are not large. Hence this method is suitable for locating the flame base which exhibits larger *axial* density gradients and relatively smaller *radial* density gradients. The momentum equation was transformed into an ordinary differential equation and solved by direct integration. Differing from the approach in the available literature, the momentum equation includes a buoyancy term. The Grashof number associated with the buoyancy is assumed to be constant throughout region 2.

The energy equation and its solution inside the laser beam is given below.

Energy

$$\rho C_p \bar{U}\frac{\partial T}{\partial x} = \frac{\partial}{r\partial r}\left(\kappa r\frac{\partial T}{\partial r}\right) + q \tag{21}$$

where

$$q = q_0[1 - \mathrm{e}^{(-\alpha_{abs}P\Delta L)}] - \frac{\varepsilon\sigma(T^4 - T_{ref}^4)}{L}. \tag{22}$$

Temperature profile

$$T(x,r) = \frac{C_3}{2x}\mathrm{e}^{-Ur^2/4\alpha x} + \frac{\alpha q}{U\kappa}x + C_4. \tag{23}$$

The energy equation has a source term which is balanced by convection and by radial heat conduction. The radiation is also taken into account by subtracting the amount of energy radiated by the silicon particles from the amount of energy absorbed from the CO_2 laser beam.

5.3.3. *Region* 3: *Downstream of the reaction zone.* The equations governing the post-reaction region are similar to the ones developed for laser-heated region 2 except that they do not have any source terms. The Grashof number in this region has been set to zero since the surrounding argon gas has also been heated through conduction and radiation. The source term in energy equation (21) is also zero because there is no interaction with the laser beam. The resulting expressions for the velocity and the temperature expressions are given as

$$u = \frac{vf'}{x\eta} \tag{24}$$

where f' is a similar expression (different constant of integration) as equations (20) and (22) but with $Gr = 0$

$$T = \frac{C_5}{2x}\mathrm{e}^{-ur^2/4\alpha x} + C_6. \tag{25}$$

Boundary conditions

$$T(\infty, 0) = T_w$$

$$T(x, \infty) = T_w$$

$C_0, C_1, C_2, C_3, C_4, C_5, C_6$ are constants of integration.

5.4. *Calculation procedure*

The solutions and their derivatives, developed for zones 1, 2 and 3, are equated at the common boundaries of these subregions. By using the patching procedure and the boundary conditions, it is possible to determine all the integration constants except C_2. The value of C_2 is obtained through balance between the net amount of energy absorbed and convected

$$q = 2\pi\int_{vol}\rho C_p\left(\frac{\partial T}{\partial x}\right)ur\,\mathrm{d}r\,\mathrm{d}x \tag{26}$$

where C_2 is defined within the expression for 'u' above.

The following summarizes the calculation steps.

(1) The energy source term without radiation is calculated.

(2) The integration constants C_1, C_3, C_4, C_5, C_6 of the temperature solutions are obtained.

(3) The energy source term is corrected for radiation.

(4) The new temperature field is calculated.

(5) The velocity source term is calculated.

(6) The integration constants for velocities C_0 and C_2 are calculated.

(7) The velocity field is evaluated.

Several more iterations can be made between steps 2–7 given above.

6. RESULTS AND DISCUSSION

Axial and radial temperature and velocity profiles were obtained for different run conditions (Table 1).

Two main parameters were systematically changed throughout the theoretical runs: the cell pressure and the silane mass flux. First the cell pressure was varied from 0.2 to 0.7 atm. Figures 6 and 7 represent the corresponding axial velocity and temperature distributions. The two lower curves in Fig. 6 correspond to a cell pressure of 0.7 atm. The slower the velocity, the longer the residence time in the laser beam. Consequently this leads to higher peak temperatures (Fig. 7). A second set of curves has been plotted on Figs. 6 and 7 where the silane mass flow rate has been decreased to 30 $cm^3\ min^{-1}$ STP. This new condition produces smoother velocity gradients in the reaction zone but also sharper axial temperature gradients. As can be seen from Fig. 7, the predicted temperatures do not agree well in preheat region 1.

This has two probable causes. First the initial temperature exiting the nozzle was taken to be 30 K (room temperature) and this value is probably too low because of the proximity of the reaction zone. The axial heat conduction and radiation from the flame will increase the nozzle temperature, thus shifting the temperature curve upward. Second, too few terms may have been retained in the series solution of region 1. As the pressure is increased from 0.2 to 0.7 atm, the velocity drops by a factor of about 4 while the temperature merely increases by a factor of 1.1 (Figs. 6 and 7). This phenomenon can be explained by examining the groups of parameters which have emerged from the solutions (equations (10)–(25)). Thus the velocity in the reaction zone depends on the dimensional group $\mu/\rho x$ (equation (18)) and the dimensionless group $Gr^{1/2}\eta^2/8$ (equation (20)). In contrast, the temperature in region 2 depends on the dimensional group $(\alpha q x/U\kappa)$ and the dimensionless group $(Ur^2/4\alpha x)$ (equation (23)). Hence the velocity is inversely proportional to density (and pressure) while for the temperature solution (equation (21)), the density change affects both the numerator (through velocity $U \sim 1/\rho$) and the denominator (through the thermal diffusivity coefficient α). Thus a change in density affects the velocity more than the temperature field. Figure 8 is a radial velocity plot at 0.2 atm and 38 $cm^3\ min^{-1}$ silane. Argon–silane gas mixing was neglected so that the decrease of the velocity is primarily due to the widening of the silane jet. Figures 9 and 10 are different plots of the same temperature data (0.2 atm, 38 $cm^3\ min^{-1}$ silane). The experimental radial velocity and temperature curves are not reported here because the probe support system was not suitable for a radial sweep of the flow field. However, the velocity and temperature measurement techniques presented in this paper are readily adaptable for such purposes.

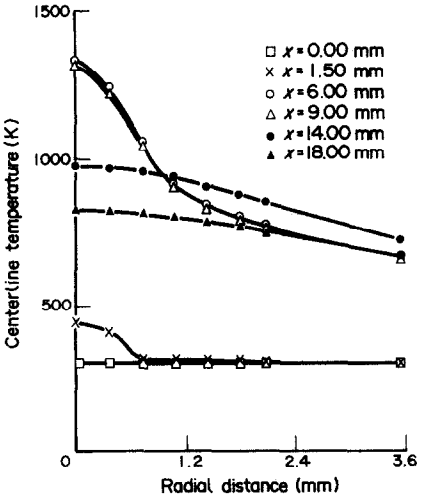

FIG. 9. Radial temperature profiles.

7. CONCLUSION

The pyrolysis of the silane jet co-flowing with an annular argon gas has been modeled with asymptotic closed form solutions. Axial velocity and temperature profiles have been measured and plotted along with the analytical results. The main advantage of doing such modeling, is to evaluate the effect of important parameters such as the cell pressure and the silane

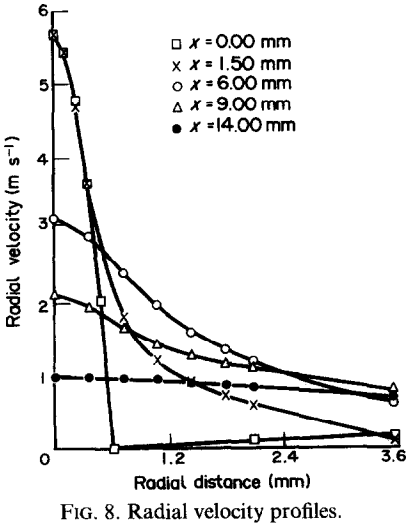

FIG. 8. Radial velocity profiles.

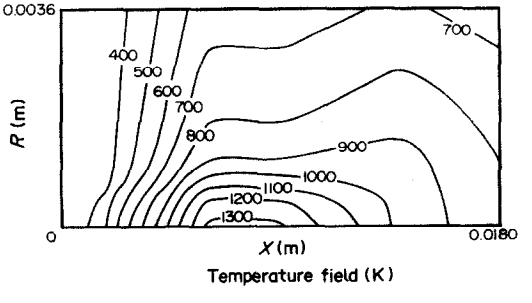

FIG. 10. Temperature map of the reaction zone.

mass flux. Also a comparison between experimental and theoretical results revealed the following.

(1) In the reaction zone, the velocity decreases due to the combined effect of heated gas expansion and the production of 2 mol of hydrogen gas for 1 mol of silane. In the theoretical curve, the velocity decrease is more pronounced than the one in the experimental curve because no argon flow mixing has been assumed. Therefore, the silane gas undergoes full thermal decomposition coupled with a strong hot gas expansion causing—slower than measured—centerline velocity values.

(2) Similarly, the calculated temperature values are higher than the measured one for the same reason mentioned above. The lack of argon at the centerline causes more laser photon energy to be absorbed by the silane gas and this results in a—higher than measured—peak temperature. These high temperatures are consequently being radiated to the surrounding. This loss mechanism couples with the heat conduction phenomena and causes relatively low centerline temperatures in the post-reaction zone.

These are the main differences between analytical and experimental results. However, the general trend outlined independently by these two methods shows agreement.

REFERENCES

1. H. E. Helms and P. W. Heitman, Ceramic components for the AGT 100 engine, ASME 84-GT-81 (1984).
2. M. L. Torti and S. D. Hartline, High performance ceramics for heat engine applications, ASME 84-GT-92 (1984).
3. H. E. Helms and S. R. Thrasher, Ceramic applications in turbine engines (CATE) development testing. ASME 83-GT-179 (1983).
4. K. Hagemeister, E. Tiefenbacher and P. Walzer, Ceramic components for high temperature vehicular gas turbines, ASME 83-GT-205 (1983).
5. E. M. Coltrin, J. K. Kee and A. J. Miller, A mathematical model of the coupled fluid mechanics and chemical kinetics in a chemical vapor deposition reactor, *J. Electrochem. Soc. Solid St. Sci. Technol.* 425–434 (1984).
6. T. Tau-Yi, *Combustion Dynamics, The Dynamics of Chemically Reacting Fluids*, p. 41. McGraw-Hill, New York (1983).
7. S. I. Flint, Powder temperatures in laser driven reactions, M.S. Thesis, MIT (February 1982).
8. H. Schlichting, *Boundary Layer Theory*, 7th Edn, p. 233. McGraw-Hill, Dusseldorf (1979).
9. I. S. Akmandor, Laser Doppler velocimetry: measurements in plane Poiseuille flow, pp. 39–43, M.S. Thesis, MIT (June 1982).
10. H. B. Squire, The found laminar jet, *Q. J. Mech. Appl. Math.* **IV**(3), 321–329 (1951).
11. I. S. Akmandor, Theoretical and computational models of reacting silane gas flows: laser driven pyrolysis of subsonic and supersonic jets, Sc.D. Thesis, MIT (June 1985).

TRANSFERT DE CHALEUR ET DE QUANTITE DE MOUVEMENT DANS LA DECOMPOSITION DE JETS DE SILANE INDUITE PAR LASER: THEORIE ET EXPERIENCE

Résumé—De la poudre de silicone est obtenue par la pyrolyse au laser du gaz de silane. Les profils de température et de vitesse sont déterminés expérimentalement et théoriquement. La vélocimétrie est une technique de marqueur qui mesure le temps de propagation d'un front de perturbation à travers la zone chaude de réaction. Dans le modèle théorique, l'expansion coaxiale du jet correspondant au chauffage est étudiée en définissant une transformation Dorodnitzin–Illingworth. Les résultats montrent une décroissance de la vitesse axiale lorsque le gaz entre dans la région chaude du laser. Le changement est intense pour des vitesses d'entrée élevées. Dans cette région, les gradients des profils de température sont élevés.

WÄRME- UND IMPULSTRANSPORT BEI DER ZERSETZUNG EINES SILAN-STRAHLES MIT HILFE EINES LASERS: THEORIE UND EXPERIMENTE

Zusammenfassung—Mit Hilfe der Laser-Pyrolyse wurde Silizium-Pulver aus Silan-Gas hergestellt. Temperatur- und Geschwindigkeitsprofile wurden sowohl experimentell als auch theoretisch bestimmt. Die Geschwindigkeitsmessung beruht auf einem Markierungsverfahren, bei dem die Ausbreitungszeit einer Störungsfront durch die heiße Reaktionszone gemessen wird. Im theoretischen Modell wird die koaxiale Strahlexpansion, bei der thermisch geheizt wird, durch Einführen einer Dorodnitzin–Illingworth-Transformation untersucht. Die Ergebnisse zeigen eine Abnahme der Axialgeschwindigkeit beim Eintritt des Gases in die Heizzone des Lasers. Dieser Effekt wird deutlicher mit zunehmender Eintrittsgeschwindigkeit. In diesem Bereich sind die Gradienten der axialen Temperaturprofile groß.

ПЕРЕНОС ТЕПЛА И КОЛИЧЕСТВА ДВИЖЕНИЯ ПРИ ЛАЗЕРНОМ РАЗРУШЕНИИ СИЛАНОВЫХ СТРУЙ: ТЕОРИЯ И ЭКСПЕРИМЕНТ

Аннотация—В результате пиролиза газа силана в лазерном излучении получены кремниевые порошки. Теоретически и экспериментально определены профили скорости и температуры. При определении скорости использовался метод маркировки для измерения времени распространения фронта возмущения по высокотемпературной зоне реакции. В теоретической модели расширение коаксиальной струи под воздействием теплового нагрева исследуется с помощью преобразования Дородницина–Иллингворта. Результаты показывают, что при входе газа в нагреваемую лазером область осевая скорость уменьшается. Более резкие изменения происходят в случае повышенных скоростей на входе. В этой области градиенты аксиальных профилей температур имеют высокие значения.